Quantum dots provide an optical signal specific to full collapse fusion of synaptic vesicles

Qi Zhang, Yu-Qing Cao*, and Richard W. Tsien†

Department of Molecular and Cellular Physiology, Stanford University, Stanford, CA 94305

Edited by Wolfhard Almers, Oregon Health and Science University, Portland, OR, and approved September 11, 2007 (received for review July 24, 2007)

Synaptic vesicles are responsible for releasing neurotransmitters and are thus essential to brain function. The classical mode of vesicle recycling includes full collapse of the vesicle into the plasma membrane and clathrin-mediated regeneration of a new vesicle. In contrast, a nonclassical mode known as "kiss-and-run" features fusion by a transient fusion pore without complete loss of vesicle identity and offers possible advantages for increasing the throughput of neurotransmission. Studies of vesicular traffic have benefited greatly from fluorescent probes like FM dyes and synaptopHluorin. However, intrinsic properties of these probes limit their ability to provide a simple and precise distinction between classical and nonclassical modes. Here we report a novel optical probe specific to full collapse fusion, capitalizing on the size and superior photo-properties of photoluminescent quantum dots (Qdots). Qdots with exposed carboxyl groups were readily taken up by synaptic vesicles in an activity-, Ca^{2+}-, and clathrin-dependent manner. Electron microscopy showed that Qdots were harbored within individual vesicles in a 1:1 ratio. The release of Qdots was activity- and Ca^{2+}-dependent, similar to FM dyes. As artificial cargo, ≈15 nm in diameter, Qdots will not escape vesicles during kiss-and-run but only with full collapse fusion. Strikingly, Qdots unloaded with kinetics substantially slower than destaining of FM dye, indicating that full-collapse fusion contributed only a fraction of all fusion events. As a full-collapse–fusion-responsive reporter, Qdots will likely promote better understanding of vesicle recycling at small CNS nerve terminals.

kiss-and-run | fusion pore | quantal release | electron microscopy | nerve terminal

Synaptic vesicles are small membrane-bounded organelles that fuse with the plasma membrane to release neurotransmitter, a key aspect of signaling between neurons. In full collapse fusion (FCF), the classical mode elegantly described by Heuser and Reese (1), the vesicle membrane merges completely with plasma membrane; clathrin-mediated retrieval of a similar amount of membrane ensues, tens of seconds later (2). The delayed retrieval supports regeneration of vesicles but create a temporal bottleneck, of concern for small CNS synapses containing only a few dozen recycling vesicles (3). "Kiss-and-run" (K&R) is a nonclassical mode of fusion (4) wherein vesicles fuse transiently with plasma membrane to release neurotransmitter (5) and are quickly recaptured on site without loss of shape and possibly other aspects of their identity. K&R and reuse of recaptured vesicles could provide a valuable complement to FCF for efficient use of vesicles (3, 6).

Studies of fusion modes and their possible importance have benefited greatly from optical probes. Styryl dyes like FM1-43 fluoresce brightly when harbored in the hydrophobic vesicle membrane, but not in aqueous solution, and thereby report vesicle fusion events (7). SynaptopHluorin (Syn-pH) displays a pH-sensitive fluorescent domain in the vesicle lumen to monitor fusion-generated pH shifts. These probes focus on particular aspects of fusion events, involving lipids or vesicular proteins (8), and have supplied valuable insights into vesicle dynamics. However, neither FM dyes nor Syn-pH provide a signal that crisply distinguishes K&R from FCF. FM dye can leave the vesicle membrane by various routes, by aqueous departitioning and escape through the fusion pore during K&R (9, 10), or by lateral diffusion away from fused membrane upon FCF (11). Clusters of vesicular Syn-pH can persist in two ways, corralled in the vesicle during K&R, or tethered by auxiliary proteins even after FCF (12). Furthermore, these probes are not responsive to vesicle shape, the fundamental factor in the original definitions of FCF and K&R (1, 4, 5).

We sought an approach to discriminate sharply between FCF and K&R, focusing on this fundamental distinction: the degree of opening of the vesicle lumen. Inspired by the finding that chromaffin granules use K&R to release small molecules (catecholamines) and FCF to discharge their dense peptide core (13), we chose quantum dots (Qdots) as a promising artificial cargo. Extremely bright and photostable, Qdots have been widely used in studies requiring high signal-to-noise ratio (14), for example, studies of the lateral diffusion of glycine and AMPA receptors (15–17). Like probes for sizing the pores of ion channels (18), Qdots could gauge the narrowest aperture in the path between vesicle lumen and external medium, escaping only if the vesicle undergoes drastic loss of shape, i.e., FCF. In examining Qdots with favorable spectral properties, emission at 605 nm, we realized that their ≈15 nm size was ideal: small enough for a Qdot to fit into a synaptic vesicle, but large enough to be completely rejected by K&R fusion pores (1–5 nm) (19).

Results

Synaptic Boutons Take Up Qdots. The emission spectrum of Qdots emitting at 605 nm fits neatly between those of EGFP and FM4-64 [supporting information (SI) Fig. 6], allowing concurrent visualization of Qdots and the other optical probes. With an organic coating bearing carboxyl groups, the Qdots had an equivalent hydrodynamic diameter of 15.0 ± 0.3 nm, measured by quasi-elastic light scattering (Y. Li and P. Strop, personal communication). To test whether Qdots might be loaded into synaptic vesicles, cultured hippocampal neurons were exposed to 400 nM Qdots and stimulated at 10 Hz for 2 min, a stimulation protocol widely used to mobilize the total recycling pool of vesicles (TRP) (20). Extensive washing for 10–15 min revealed isolated photoluminescent puncta resembling synaptic boutons (Figs. 1*A* and 2*A*). To characterize these bright puncta, we later stained the same neurons with FM4-64, an established label for functional synaptic vesicles. A near perfect overlap of Qdot and FM4-64 signals was found (96.1%, determined with ImageJ as the proportion of Qdot-positive pixels covered by an FM4-64-positive pixel mask) (Fig. 1*A*). We also fixed

Author contributions: Q.Z., Y.-Q.C., and R.W.T. designed research; Q.Z. and Y.-Q.C. performed research; Q.Z., Y.-Q.C., and R.W.T. analyzed data; and Q.Z. and R.W.T. wrote the paper.

The authors declare no conflict of interest.

This article is a PNAS Direct Submission.

Freely available online through the PNAS open access option.

Abbreviations: FCF, full collapse fusion; K&R, kiss-and-run; Qdot, quantum dot; ROI, region of interest.

*Present address: Department of Anesthesiology, Washington University Pain Center, St. Louis, MO 63110.

†To whom correspondence should be addressed. E-mail: rwtsien@stanford.edu.

This article contains supporting information online at www.pnas.org/cgi/content/full/0706906104/DC1.

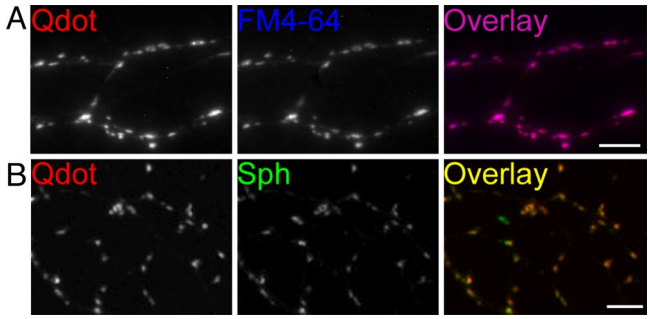

Fig. 1. Qdots are colocalized with markers for presynaptic vesicles. (*A*) Qdot labeling (red) and subsequent FM4-64 staining (blue) display almost complete overlap (purple). (Scale bar, 5 μm.) (*B*) Qdot signals (red) show near-complete overlap with synaptophysin staining (green). (Scale bar, 5 μm.)

hippocampal neurons loaded with Qdots and immunolabeled synaptophysin, a well known marker for synaptic vesicles. Again, we observed almost complete overlap (95.3%) (Fig. 1*B*). These findings agreed in indicating that Qdots were taken up by synaptic boutons.

Qdot Surface Coating Influences Membrane Interaction and Uptake. At a loading concentration of 400 nM, the number of Qdots in a vesicle's worth of free solution is far too low to account for Qdot internalization by random engulfing of external fluid. What raises the chances of Qdot uptake? Surface interactions were clearly important. Qdots with carboxyl-exposed coating bound to neuronal processes in strong preference to neighboring glia (SI Fig. 7*A1*). The affinity for neuronal membrane was not seen with similar Qdots that had been surface rendered with polyethylene glycol (PEG) with little change in size (SI Fig. 7*B1*). The influence of surface coating was studied by imaging during the wash after Qdot loading (SI Fig. 7*C*). Even after extensive washing, Qdots were largely retained at synaptic boutons, reflecting Qdot internalization (SI Fig. 7*A2*). Very different results were obtained with PEG-coated Qdots (400 nM, SI Fig. 7*B*). No neuron-specificity was seen, and Qdots at presynaptic regions were completely removed by washing, showing a prior lack of internalization (SI Fig. 7*B2*). The difference between the two types of Qdots was further indicated by their off-rates from nonpresynaptic regions of neuronal membrane (SI Fig. 7*C2*). In contrast to the slow removal of carboxyl-bearing Qdots, PEG-coated Qdots washed away much faster. Thus, surface properties influenced Qdot affinity, off-rate, and propensity for synaptic uptake.

Membrane-attached particles can enter cells by phagocytosis or constitutive endocytosis, independent from synaptic vesicle retrieval. We next asked whether Qdot uptake had hallmarks of synaptic vesicle cycling, namely activity-evoked, Ca^{2+}-dependent, and clathrin-mediated endocytosis. First, we noted that exposure of quiescent neurons to Qdots led to a much more diffuse pattern of photoluminescence along the neuronal membrane, which could be eliminated with a 10-min wash (data not shown). Second, the amount of Qdot a synaptic bouton could take up was strongly correlated with the intensity of subsequent FM4-64 staining (Fig. 2*B*), again supporting the notion that Qdots entered synaptic vesicles during exo-endocytotic cycling. Withdrawal of external Ca^{2+} during stimulation resulted in virtually no Qdot signal at synaptic boutons no matter how much FM4-64 those boutons took up after $[Ca^{2+}]_o$ had been restored (Fig. 2 *A* and *B*).

To investigate the clathrin-dependence of Qdot loading, we used a genetically encoded blocker for clathrin-mediated endocytosis,

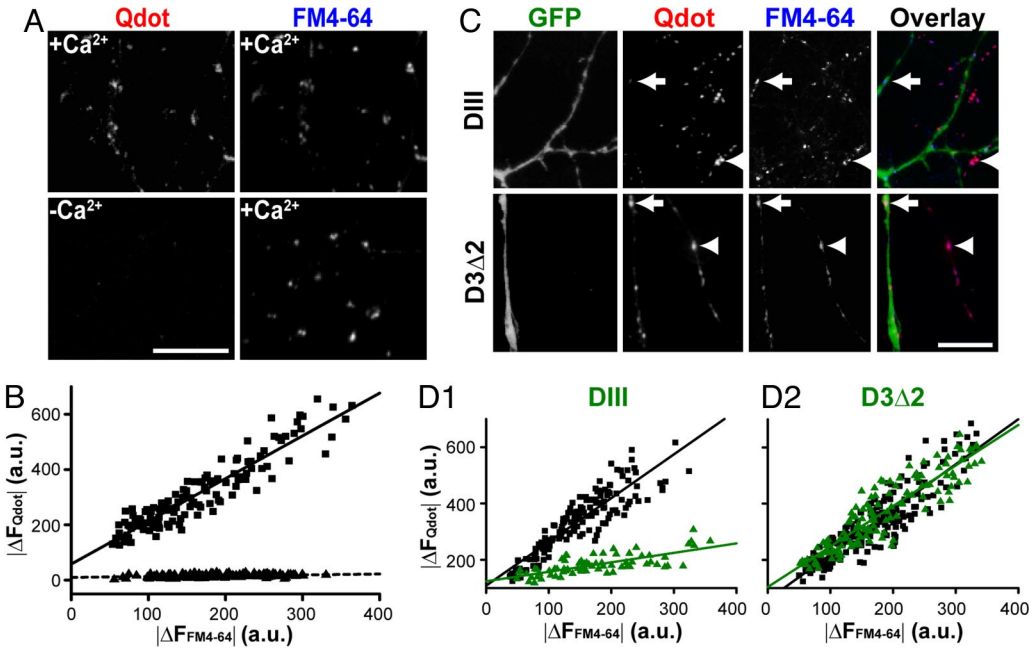

Fig. 2. Qdot uptake is Ca^{2+}-dependent and clathrin-mediated. (*A*) (*Left*) Qdot loaded in the presence (*Upper*) or absence (*Lower*) of Ca^{2+}. (*Right*) FM4-64 loaded in the same fields (4× 10-Hz 2-min stimulation) in the presence of Ca^{2+}. (Scale bar, 10 μm.) (*B*) The relationship between Qdot loading ($|\Delta F_{Qdot}|$) and FM4-64 staining ($|\Delta F_{FM4\text{-}64}|$) is significantly different depending on the presence of Ca^{2+} during loading (squares) or the absence (triangles) ($P < 0.001$, Kolmogorov–Smirnov test). Each data point represents an individual ROI. (*C*) EGFP fluorescence reveals neurons expressing DIII-EGFP or D3Δ2-EGFP, and retrospective FM4-64 staining marks functional boutons. Boutons of DIII–EGFP expressing neurons (arrow) take up Qdots to a significantly lesser degree than those of nontransfected neurons (arrowhead). Boutons of neurons expressing D3Δ2-EGFP (arrow) take up Qdots similarly to those of nontransfected neurons (arrow head). (Scale bar, 5 μm.) (*D1* and *D2*) The relationship between Qdot loading ($|\Delta F_{Qdot}|$) and FM4-64 staining ($|\Delta F_{FM4\text{-}64}|$) is significantly different for DIII-EGFP expressing neurons (green triangles) and nonexpressing neurons in the same culture (black squares) (*D1*, $P < 0.001$, Kolmogorov–Smirnov test). Expression of the inactive D3Δ2-EGFP (green triangles) gives no significant difference from nonexpressing control neurons (black squares) (*D2*, $P > 0.5$, Kolmogorov–Smirnov test). Note that FM4-64 staining was spared under all circumstances, likely because 4× high K^+ stimulation was greatly supermaximal for loading and dye could load even with K&R.

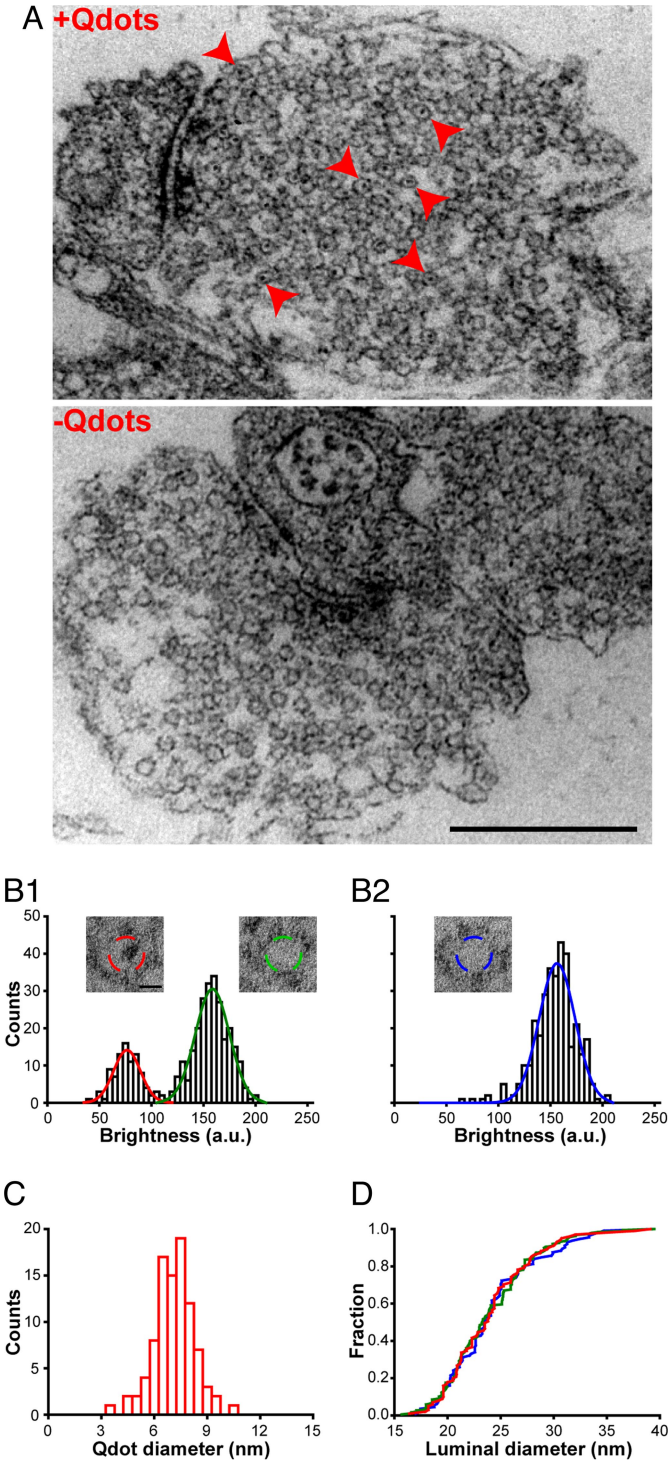

Fig. 3. Only one Qdot is localized in the lumen of one synaptic vesicle. (*A*) Samples of Qdot-loaded synapse (+Qdots) and control (−Qdots). Red arrowheads point to vesicles containing electron dense puncta. (Scale bar, 500 nm.) (*B*) Distributions of luminal intensities (ROI indicated by dashed circles in *Insets*) of vesicles from four Qdot-loaded synapses (*B1*) and four control synapses (*B2*), with sum-of-Gaussian fits. A separate peak (red curve) is obvious in *B1*. (*Insets*) Exemplars of Qdot-positive vesicles and Qdot-negative vesicles at Qdot-loaded synapses and vesicles at control synapse. (Scale bar, 10 nm.) (*C*) Distribution of the diameters of electron dense puncta in vesicles at Qdot loaded synapses. (*D*) Cumulative distribution of inner diameters of Qdot-containing vesicles (red), empty vesicles in Qdot-loaded synapses (green), and vesicles in control synapses (blue). No significant differences (Kolmogorov–Smirnov test, $P > 0.1$ for red vs. green, and $P = 0.9$ for red vs. blue) were observed.

the AP-2 binding domain of Eps15 (DIII). Overexpression of DIII prevents endogenous Eps15 from binding to AP-2 and thus disrupts clathrin-mediated endocytosis (21). Boutons expressing EGFP tagged-DIII (cDNA kindly provided by A. Benmerah, Institut Cochin, U. Paris Descartes, Paris, France) took up significantly fewer Qdots comparing to nontransfected ones in the same culture (Fig. 2 *C* and *D*). Again, the vitality of boutons was confirmed by FM4-64 staining. In contrast, EGFP tagged-D3Δ2, a DIII mutant lacking AP-2 binding ability (21), had no effect on Qdot uptake (Fig. 2 *C* and *D*). Taken together, these findings indicated that Qdot uptake was associated with clathrin-mediated membrane retrieval after synaptic activity.

Qdots Reside in Synaptic Vesicles. Apart from generating synaptic vesicles, engulfed lipid membrane can merge with endosome/cisternae, or possibly contribute to sparsely distributed dense core vesicles (22). Thus, it was essential to determine whether membrane-bound Qdots ended up in synaptic vesicles or in other lipid compartments. Qdots can be detected by electron microscopy (EM) because their core-shell structure consists of CdSe and ZnS, suitably electron dense material (23). Capitalizing on this advantage, we processed neurons for EM after confirming the success of Qdot loading with light microscopy. EM revealed that after whole bouton Qdot loading (400 nM Qdot, 1,200 stimuli), 26.4 ± 8.6% ($n = 4$) of the synaptic vesicles contained an electron dense punctum (Fig. 3*A*). On the other hand, endosome/cisternae and dense core vesicles were rare structures after field stimulation (data not shown), as described in refs. 22 and 24. The dark puncta found within vesicles were often oblong rather than round, consistent with the fact that the core-shell structure of Qdots is ellipsoid in shape (4 nm × 9.4 nm according to Invitrogen documentation). The puncta were generally positioned somewhat off-center of the vesicular lumen, conforming to the notion that their outer organic coating (invisible by EM) might associate with a portion of the vesicular membrane.

For quantitative analysis, we surveyed EM images with fixed circular regions of interest (ROIs) (20 nm in diameter, sized to fit within the lumen of nearly all vesicles). Within the ROIs, the luminal brightness clearly exhibited a two-peak distribution (Fig. 3*B1*). Three-fourths of the vesicles displayed a clear lumen and conformed to a Gaussian distribution like that derived from control terminals not exposed to Qdots (Fig. 3*B2*). All of the remaining vesicles belonged to a second Gaussian distribution of lower luminal brightness, there being no third peak. Moreover, the size of the punctum (measured with a circular ROI just accommodating it in entirety) averaged 7.16 ± 0.99 nm (Fig. 3*C*), in reasonable agreement with the expected apparent size of the electron dense core-shell viewed from random angles. Both the single-peaked distribution of dark puncta inside the lumen and their apparent size supported the conclusion that individual vesicles took up at most one Qdot. The proportion of Qdot-loaded vesicles, ≈26%, was consistent with the fraction of vesicles that take up FM1-43 (3). Further analysis of the size of punctum-containing vesicles indicated that their distribution of luminal diameters was not detectably different from that of punctum-free vesicles, in either Qdot-loaded or control synapses (Fig. 3*D*). Thus, synaptic vesicles were not detectably enlarged by loading with Qdots.

We also used light microscopy to obtain a distinct estimate of the number of Qdot-loaded vesicles in single synaptic boutons. With the same imaging settings, the Qdot signal of whole boutons were compared with those of individual Qdots dispersed in agarose gel (all signals corrected for background). The average bouton intensity was found to be ≈30 times larger than the single Qdot intensity (SI Fig. 8). Given that vesicles contained either 0 or 1 Qdot, the mean number of Qdot-loaded vesicles was ≈30. Reassuringly, this value was close to the number of vesicles that have been found to take up FM1-43 with the same stimulation protocol (9, 24). Given that Qdots are too large to pass through fusion pores of sizes expected

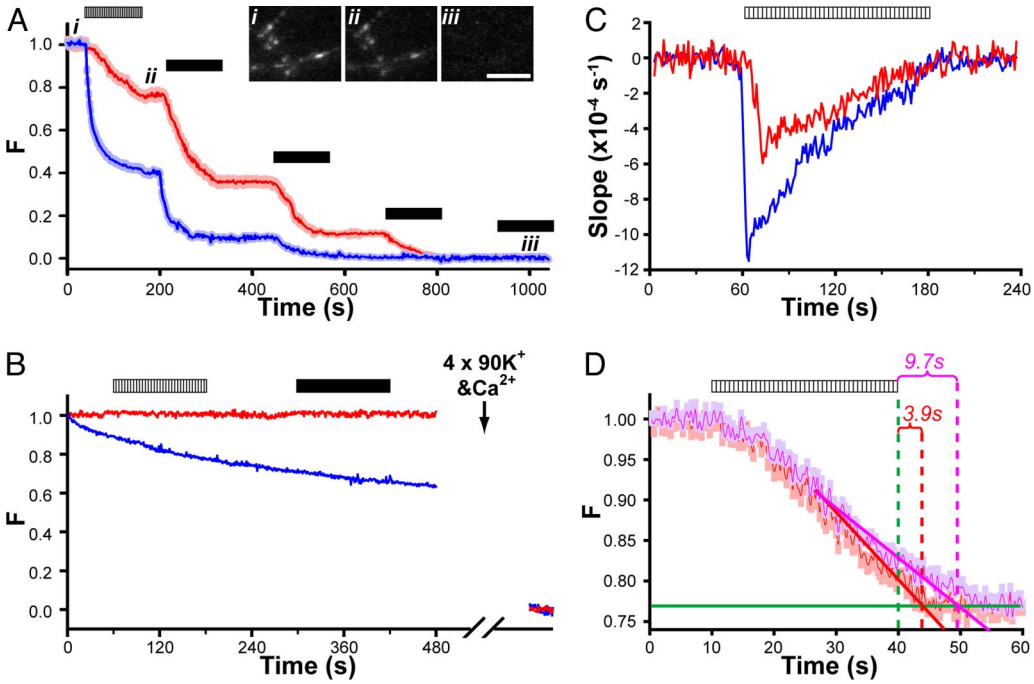

Fig. 4. Similarities and differences between Qdot unloading and FM4-64 destaining. (*A*) Multiple challenges (field stimulation, hatched bar; 2-min exposure to 90 mM K^+, black bars) each evoke Qdot loss. Images for Qdot and FM4-64 taken every other second from the same field. Intensities of both FM4-64 and Qdots were normalized to range between 1 (prestimulation baseline) and 0 (poststimulation baseline). Insets show three Qdot images taken before (*i*), after field stimulation (*ii*), and after repeated high K^+ perfusion (*iii*). (Scale bar, 5 μm.) (*B*) In the absence of extracellular Ca^{2+}, neither field stimulation (hatched bar) nor 90 mM K^+ (black bar) caused any Qdot loss (red trace). Similar results were found for FM4-64 (blue trace), but with prominent photobleaching. At far end of time axis are averaged signals from the same boutons after 4× high K^+ challenge with Ca^{2+} present. The intensity values are normalized as in *A*. (*C*) The average slopes of Qdot unloading (red) and FM4-64 destaining (blue) with field stimulation. Qdot slope shows a delayed (≈10 s) onset and 2-fold lower peak, reflecting slower Qdot release from boutons. (*D*) Speed of Qdot escape from collapsed vesicle is relatively rapid even with whole bouton loading. A 10-Hz field stimulation ceased after 30 s and four rounds of high K^+ Tyrode were used after >1 min rest to empty the remaining Qdots from synapses. Slanted lines fitted Qdot photoluminescence data over the last 15 s of stimulation (solid red line for 9-pixel ROIs; pink line for 17-pixel ROIs) and horizontal lines (solid green) fitted data 30–60 s after stimulation. These lines intersected ≈3.9 s (and 9.7 s) after termination of field stimulation (30 s). Qdot signals were normalized as in *A*.

for K&R (1–3 nm), the agreement suggests that all recycling vesicles will eventually undergo FCF.

Unloading of Qdots is Activity-Evoked and Ca^{2+}-Dependent. To be an effective reporter for vesicle turnover, loaded Qdots needed to be releasable from host vesicles via activity-driven exocytosis. With constant solution flow, such Qdot release should be seen as a loss of Qdot photoluminescence from synaptic boutons. Indeed, we observed that field stimulation (10 Hz, 2 min) caused Qdot photoluminescence to drop, in step with stimulation-evoked FM4-64 loss from the same boutons (Fig. 4*A*). Similar to FM4-64, Qdot intensity was further reduced by repeated high K^+ challenges to a level indistinguishable from background, indicating a complete loss of Qdots after extensive stimulation (Fig. 4*A*). Removal of external Ca^{2+} abolished Qdot loss with either field stimulation or high K^+ challenges (Fig. 4*B*); in this circumstance, Qdot intensity showed no decay during minutes of imaging, reflecting its extreme photostability, whereas the fluorescence of FM4-64 continuously decreased due to photobleaching. The stimulation-evoked and Ca^{2+}-dependent uptake and loss of Qdots supported the hypothesis that these nanoparticles can enter and exit synaptic vesicles via the classical mode of vesicle turnover.

Qdot Loss Selectively Reported FCF Without Compromise of Neurotransmission. Intriguingly, the kinetics of Qdot loss clearly differed from that of FM4-64, in displaying a lower initial rate and slower time course (Fig. 4 *A* and *C*). The peak speed of Qdot loss was ≈52% of the maximal rate of FM4-64 loss (Fig. 4*C*), and overall, the extent of Qdot loss was significantly less than that of FM4-64. Could this disparity indicate that Qdot-detectable FCF comprised only a fraction of all fusion events? Before considering this idea, we systematically examined various factors that might influence the rate of Qdot loss, namely (*i*) the number of recycling vesicles that Qdots can access, (*ii*) the release probability (P_r) of Qdot-loaded vesicles, and (*iii*) the efficiency of Qdot departure once vesicles have fully flattened.

First, as already noted, the average number of Qdot-accessible vesicles per bouton, determined by either light or electron microscopy (Fig. 3 and SI Fig. 8), was no different from the number of vesicles in the total recycling pool, previously estimated by FM1-43 methods (3, 25). This finding indicated that Qdots, like FM1-43, labeled the whole TRP. Second, any influence of Qdots on the probability of fusion (P_r) would not have accounted for the disparity shown in Fig. 4*A*, because FM dye loss and Qdot unloading were studied in the same boutons. To look specifically for an effect of Qdots on P_r or the prevalence of fusion modes, we compared the rate of FM4-64 destaining in the presence and absence of Qdots, noting that FM dye loss depends strongly on both P_r and fusion mode (9, 10, 27). No difference was observed (Fig. 5 *A* and *B*), weighing against changes in P_r or in fusion mode prevalence. Moreover, electrophysiological recordings of evoked postsynaptic current (EPSC) at autaptic synapses showed no significant differences in EPSC amplitude at Qdot-loaded and sham-treated control synapses ($P > 0.05$, Fig. 5*C*). These observations indicated that Qdots had no adverse influence on P_r. As a third possibility, we considered the scenario wherein all vesicles fuse by FCF, but Qdots linger at the already-flattened membrane for long enough to be recaptured by endocytosis. The kinetics of Qdot departure from the ROI after exocytosis could be derived from data after sudden cessation of field stimulation (Fig. 4*D*). If escape of Qdots from the

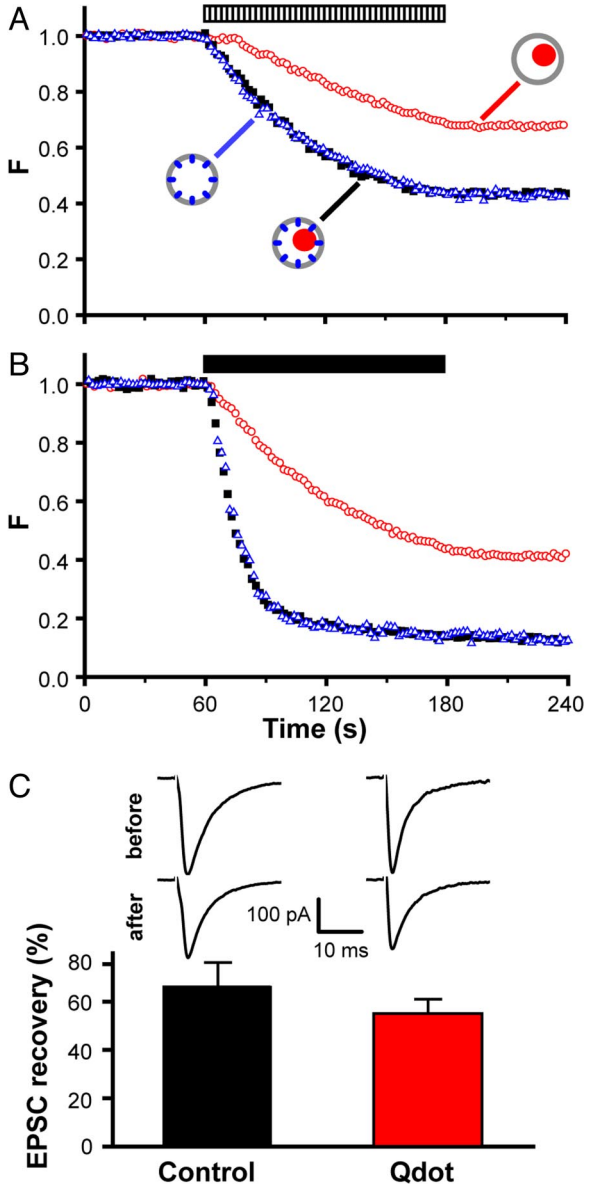

Fig. 5. Qdots exert no discernable influence on neurotransmission. (*A* and *B*) Fluorescence or photoluminescence changes of FM4-64 or Qdot during field stimulation (hatched bar) or high K^+ challenge (black bar). Data represent three loading conditions, Qdots only (red circles), FM4-64 only (blue triangles), or FM4-64 at Qdot co-loaded boutons (filled black squares). Intensities of photoluminescent/fluorescent signals normalized as in previous figures. (*C*) Samples of EPSCs recorded before and after Qdot loading or from sham control. Ratio of EPSCs recorded after and before Qdot loading (recovery/baseline). No significant difference between Qdot-loaded and sham control neurons ($P > 0.25$, *t* test).

ROI had been instantaneous, the near-linear decline in light output would have stopped abruptly when stimulation ceased. In fact, the optical signal continued to decrease for a short period after the end of a 30-s 10-Hz stimulation (t_{end}). An extrapolation of the linear decline crossed the final baseline ≈3.9 s after t_{end}, thus indicating how long photoluminescence loss can be expected to lag stimulus-induced exocytosis for an ROI of 1.3 μm. We conducted a similar measurement with larger ROIs, 17 pixels (2.5 μm) in diameter. In this case, the extrapolated linear decline intercepted the baseline 9.7 s after t_{end}. The extra delay was roughly as expected for lateral diffusion of Qdots after exiting from the vesicular lumen, out of the presynaptic area and into nearby axonal membrane outside of the ROI, where slower dissociation could take place. Delays originating from lateral movement cannot account for the overall difference in the slopes of the FM dye and Qdot signals. In addition, we considered the notion that Qdots that undergo FCF might be endocytosed without ever leaving the ROI, but concluded that the surface concentration of externalized Qdots would be too low for this to be a significant factor (SI Fig. 7). Thus, the remaining discrepancy between the optical signals must be attributed to a size-based discrimination by Qdots, which are expected to escape the vesicle and ROI following FCF, but not with K&R. According to this interpretation, the initial proportion of K&R events must be ≈50% or greater. A more precise determination may be derived by tracking single Qdots taken up into individual vesicles (Q.Z. and R.W.T., unpublished data).

Discussion

Qdots with exposed carboxyl groups bound to neuronal membranes and were endocytosed into synaptic terminals during neuronal activity. Under EM, the Qdots were seen as dark puncta within individual vesicles in a 1:1 ratio. Qdots caused no obvious disruption in vesicle morphology or neurotransmission. The Qdots were released from nerve terminals in an activity- and Ca^{2+}-dependent manner as expected for vesicles undergoing FCF. The rapid halting of photoluminescence loss just after cessation of stimulation indicated that externalized Qdots escaped quickly ($\tau < 4$ s) from the region of interest, most likely by lateral movement out of the ROI.

Qdots have superior physical features, well suited to clarifying vesicle fusion modes. We took advantage of their size, much too large to pass through fusion pores of K&R (1–5 nm). Instead, Qdots will only exit synaptic vesicles when the connecting pathway to the external medium exceeded ≈15 nm, approaching the size of the vesicular lumen itself (≈24 nm), and thereby committing the vesicle to FCF. Thus, escape of the Qdot marks FCF only. As clathrin assembly and membrane retrieval after FCF requires tens of seconds (26), several fold longer than the lag for Qdot escape ($\tau <$ 4 s), FCF events will be reported by Qdots with near-perfect fidelity. Given this selectivity for FCF, it was striking to find that Qdots reported significantly fewer fusion events than concurrent destaining of FM dye. The discrepancy would have been greater still if FM dye destaining had been fast enough to report all fusion events perfectly (9, 10, 27). Thus, the proportion of nonclassical fusion events must have been substantial.

Another interesting finding was that synaptic vesicles can take up a sizeable "cargo" while maintaining their overall morphology and release dynamics. EM revealed no significant increase in diameter of vesicles that engulfed Qdots, suggesting that mechanisms controlling vesicle morphology had largely prevailed. Furthermore, extensive Qdot loading did not detectably reduce neurotransmission. In principle, the internalized Qdots would displace ≈1/4 of the luminal volume. Although EPSC amplitude was not correspondingly decreased, such a change may not have been discerned because of variable rundown of EPSCs, or offsetting changes in vesicle diameter, sufficient to affect transmitter content but too small to detect. It would be interesting to test whether uptake of larger Qdots can displace enough neurotransmitter to cause a clear electrophysiological change.

Qdots provide several novel opportunities for future studies of presynaptic cell biology. Because Qdots are bright but indivisible, and provide superior signal-to-noise ratios, they may allow labeling and tracking of single vesicles. In turn, this may allow presynaptic fusion modes to be related to quantal transmission. Our data point the way for use of light microscopy and EM to localize Qdot-loaded vesicles in combination with immunocytochemistry (23). Qdots of different colors could be used to track exchange between different vesicle pools within a single nerve terminal (28) or between vesicles in neighboring presynaptic terminals (29).

Methods

Cell Culture and DNA Transfection. Hippocampal CA3-CA1 neurons were cultured from P0 or P1 rats as described in ref. 30 with minor modifications. All experiments were approved by Administrative Panel on Laboratory Animal Care at Stanford University. Expression of exogenous fusion proteins in cultured neurons was achieved by calcium phosphate-mediated transfection at 10 or 11 days *in vitro* (DIV). Between 12–21 DIV, healthy cultures that met our rigorous standards (9) were selected for experiments.

Qdots and Chemicals. All Qdots were obtained from Quantum Dot Corporation (now part of Invitrogen, Carlsbad, CA) as concentrated stock solution at 8 μM. To remove congregated Qdots, stock solution was centrifuged in 4°C at $\geq$10,000 g for 15 min, then purified via size exclusion column (Superdex 200). The concentration of the resulting solution was $\approx$1.5 μM. All chemicals were obtained from Sigma (St. Louis, MO) unless stated otherwise.

Immunocytochemistry and Confocal Imaging. Cells were fixed with 4% paraformaldehyde and immunocytochemistry was performed as described in ref. 31. Samples were mounted with Vectashield mounting medium (Vector Laboratories, Burlingame, CA), and imaged on a Zeiss LSM510 confocal with a $\times$40 objective (optical section 0.5 μm). Average intensity projections $\approx$10 μm thick were used to create final images.

Real Time Imaging. Cells were usually perfused with Tyrode solution (containing 150 mM NaCl, 4 mM KCl, 2 mM $CaCl_2$, 2 mM $MgCl_2$, 10 mM glucose, 10 mM Hepes, 310–315 mOsm, with pH set at 7.35 with NaOH). High K^+ solution (90 mM K^+) was prepared by equimolar replacement of NaCl by KCl. For Ca^{2+}-free experiments, 2 mM $CaCl_2$ in the external solution was replaced by 2 mM Na-EGTA. Switching of perfusion solution was carried out with a precision of $<$2 s. All solutions contained 10 μM NBQX and 50 μM D-APV (Tocris Bioscience, Ellisville, MO) to prevent recurrent activity and synaptic plasticity. All experiments were performed at room temperature.

All image acquisition was conducted as described in ref. 9. To avoid cytotoxic effects of UV light, Qdots were excited at 470 nm (D470–40x; Chroma, Rockingham, VT) and their emission was collected at 605 nm (D605–20m). Subsequently loaded FM4-64 was excited at 490 nm (D490–20x) and its emission was collected at 660 nm (D660–50m). For imaging of Qdots and FM4-64 together, the same filter sets were used but switched every second. All images were taken at a frame rate of 1 Hz (5- to 10-ms exposure) unless stated otherwise.

Electron Microscopy. Cells were fixed with 2% glutaraldehyde in PBS for 20 min, followed by postfixation in 1% osmium tetroxide in ddH_2O at 4°C for 1 h. Then, samples were rinsed and stained with 1% uranyl acetate in ddH_2O at 4°C for 1 h. Cells were dehydrated in a cold ethanol series and infiltrated with Durcupan ACM resin (Electron Microscopy Sciences, Hatfield, PA). Polymerization took 3–5 days at 55°C. Samples were sectioned parallel to the coverslip surface, in serial fashion on a Leica microtome VT1000s ($\approx$70 nm thick). Electron micrographs were taken on JEOL 200CXII.

Electrophysiology. Recordings of autaptic EPSCs after the Qdot loading procedure ($n = 4$) (or after a sham control, $n = 4$) ("EPSC recovery") were compared with baseline EPSC recordings from the same neurons. Qdot loading was performed with 400 nM Qdot and 10 Hz intracellular stimulation for 2 min, with blockers of postsynaptic glutamate receptors present to eliminate reverberant activity and long-term synaptic plasticity. The EPSCs were completely blocked by 10 μM NBQX and 50 μM D-APV (data not shown). After Qdot loading and before the recording of EPSC recovery, a 10- to 15-min wash with normal Tyrode free of NBQX and D-APV was performed. Near complete removal of the inhibition of glutamate receptors by such wash-off was confirmed. Stimulus artifact was omitted by blanking the current signal for 2.8 ms.

Analysis of Real-Time Imaging. All images were converted to TIFF files and analyzed off-line with MetaFlour or ImageJ. In most cases, circles with a diameter of 9 pixels ($\approx$1.3 μm) were centered on FM4-64 positive puncta as regions of interest (ROIs) covering functional boutons, typically $\approx$1 μm across. These ROIs were retrospectively projected onto Qdot images and then average intensities of Qdot photoluminescence in these ROIs were exported to an Excel file. The starting time of each frame was registered by the imaging program and recorded together with ROI intensity. Data were analyzed by Excel, Statview, and SigmaPlot, and plotted with SigmaPlot. All error bars represent standard error of the mean ($\pm$SEM).

We thank Y. Li and C. Barrett for comments on the manuscript; Y. Li and P. Strop (A. Brunger laboratory) for sharing unpublished data, X. H. Gao for consultation on quantum dots, A. Benmerah for gift of DIII and D3Δ2 constructs, and N. C. Harata and R. Y. Tsien for helpful advice. This work was supported by a grant from the National Institute of Mental Health and from the Burnett Family Foundation (to R.W.T.).

1. Heuser JE, Reese TS (1973) *J Cell Biol* 57:315–344.
2. Koenig JH, Ikeda K (1996) *J Cell Biol* 135:797–808.
3. Harata N, Pyle JL, Aravanis AM, Mozhayeva M, Kavalali ET, Tsien RW (2001) *Trends Neurosci* 24:637–643.
4. Valtorta F, Meldolesi J, Fesce R (2001) *Trends Cell Biol* 11:324–328.
5. Ceccarelli B, Hurlbut WP, Mauro A (1973) *J Cell Biol* 57:499–524.
6. Kavalali ET (2006) *Neuroscientist* 12:57–66.
7. Betz WJ, Mao F, Smith CB (1996) *Curr Opin Neurobiol* 6:365–371.
8. An S, Zenisek D (2004) *Curr Opin Neurobiol* 14:522–530.
9. Aravanis AM, Pyle JL, Tsien RW (2003) *Nature* 423:643–647.
10. Richards DA, Bai J, Chapman ER (2005) *J Cell Biol* 168:929–939.
11. Zenisek D, Steyer JA, Almers W (2000) *Nature* 406:849–854.
12. Willig KI, Rizzoli SO, Westphal V, Jahn R, Hell SW (2006) *Nature* 440:935–939.
13. Fulop T, Radabaugh S, Smith C (2005) *J Neurosci* 25:7324–7332.
14. Alivisatos AP, Gu W, Larabell C (2005) *Annu Rev Biomed Eng* 7:55–76.
15. Bats C, Groc L, Choquet D (2007) *Neuron* 53:719–734.
16. Dahan M, Levi S, Luccardini C, Rostaing P, Riveau B, Triller A (2003) *Science* 302:442–445.
17. Ehlers MD, Heine M, Groc L, Lee MC, Choquet D (2007) *Neuron* 54:447–460.
18. Hille B (2001) *Ion Channels of Excitable Membranes* (Sinauer, Sunderland, MA).
19. Jackson MB, Chapman ER (2006) *Annu Rev Biophys Biomol Struct* 35:135–160.
20. Ryan TA, Smith SJ (1995) *Neuron* 14:983–989.
21. Benmerah A, Lamaze C, Begue B, Schmid SL, Dautry-Varsat A, Cerf-Bensussan N (1998) *J Cell Biol* 140:1055–1062.
22. Sorra KE, Mishra A, Kirov SA, Harris KM (2006) *Neuroscience* 141:2097–2106.
23. Giepmans BN, Deerinck TJ, Smarr BL, Jones YZ, Ellisman MH (2005) *Nat Methods* 2:743–749.
24. Harata N, Ryan TA, Smith SJ, Buchanan J, Tsien RW (2001) *Proc Natl Acad Sci USA* 98:12748–12753.
25. Aravanis AM, Pyle JL, Harata NC, Tsien RW (2003) *Neuropharmacology* 45:797–813.
26. Mueller VJ, Wienisch M, Nehring RB, Klingauf J (2004) *J Neurosci* 24:2004–2012.
27. Harata NC, Choi S, Pyle JL, Aravanis AM, Tsien RW (2006) *Neuron* 49:243–256.
28. Rizzoli SO, Betz WJ (2004) *Science* 303:2037–2039.
29. Darcy KJ, Staras K, Collinson LM, Goda Y (2006) *Nat Neurosci* 9:315–321.
30. Liu G, Tsien RW (1995) *Neuropharmacology* 34:1407–1421.
31. Zhang Q, Pangrsic T, Kreft M, Krzan M, Li N, Sul JY, Halassa M, Van Bockstaele E, Zorec R, Haydon PG (2004) *J Biol Chem* 279:12724–12733.